Proc. 19th Winter Workshop on Nuclear Dynamics (2003) 7–15

19th Winter Workshop on Nuclear Dynamics
Breckenridge, Colorado, USA
February 8–15, 2003

Recent Results from Phobos

B.B.Back[1], M.D.Baker[2], D.S.Barton[2], R.R.Betts[6], M.Ballintijn[4], A.A.Bickley[7], R.Bindel[7], A.Budzanowski[3], W.Busza[4], A.Carroll[2], M.P.Decowski[4], E.García[6,a], N.George[1,2], K.Gulbrandsen[4], S.Gushue[2], C.Halliwell[6], J.Hamblen[8], G.A.Heintzelman[2], C.Henderson[4], D.J.Hofman[6], R.S.Hollis[6], R.Hołyński[3], B.Holzman[2], A.Iordanova[6], E.Johnson[8], J.L.Kane[4], J.Katzy[4,6], N.Khan[8], W.Kucewicz[6], P.Kulinich[4], C.M.Kuo[5], W.T.Lin[5], S.Manly[8], D.McLeod[6], J.Michałowski[3], A.C.Mignerey[7], R.Nouicer[6], A.Olszewski[3], R.Pak[2], I.C.Park[8], H.Pernegger[4], C.Reed[4], L.P.Remsberg[2], M.Reuter[6], C.Roland[4], G.Roland[4], L.Rosenberg[4], J.Sagerer[6], P.Sarin[4], P.Sawicki[3], W.Skulski[8], S.G.Steadman[4], P.Steinberg[2], G.S.F.Stephans[4], M.Stodulski[3], A.Sukhanov[2], J.-L.Tang[5], R.Teng[8], A.Trzupek[3], C.Vale[4], G.J.van Nieuwenhuizen[4], R.Verdier[4], B.Wadsworth[4], F.L.H.Wolfs[8], B.Wosiek[3], K.Woźniak[3], A.H.Wuosmaa[1], B.Wysłouch[4]

[1] Argonne National Laboratory, Argonne, IL 60439-4843, USA
[2] Brookhaven National Laboratory, Upton, NY 11973-5000, USA
[3] Institute of Nuclear Physics, Kraków, Poland
[4] Massachusetts Institute of Technology, Cambridge, MA 02139-4307, USA
[5] National Central University, Chung-Li, Taiwan
[6] University of Illinois at Chicago, Chicago, IL 60607-7059, USA
[7] University of Maryland, College Park, MD 20742, USA
[8] University of Rochester, Rochester, NY 14627, USA

Abstract. The Relativistic Heavy Ion Collider (RHIC) at Brookhaven National Laboratory has delivered the collisions between Au nuclei at the highest center of mass energies achieved in the laboratory to date. PHOBOS is one of four experiments studying the these interactions. In this paper we will briefly describe the PHOBOS experiment, and discuss some of the current physics results obtained at $\sqrt{s_{NN}} = 56$ and 130 and 200 GeV: the systematic study of charged particle multiplicity as a function of pseudorapidity and centrality, measurements of anti particle to particle ratios, and the hadron spectra as function of transverse momentum for both high and low p_t.

Keywords: heavy-ion collisions, charged particle multiplicity, centrality dependence, particle anti particle ratio, charged hadron spectra
PACS: see, 25-75.q,25-75.Ld,25.75.Dw

1. Introduction

The fundamental theory of strong interactions predicts that the Quark-Gluon Plasma (QGP) will be formed for hadronic systems at sufficiently high energy density [1]. The QGP is the state of matter that previously existed about 10 micro-seconds after the Big Bang, and is a conglomerate of free quarks and gluons. The goal of the relativistic heavy ion program over the past two decades has been to find the signatures of the formation of the QGP. From data collected at the AGS, the SPS and so far from RHIC, it is clear that the search for the QGP will require a systematic effort of the entire heavy ion physics community. In this paper we survey PHOBO's contribution to this task.

The data described in this paper were taken from the RHIC 2000 run, Au+Au at $\sqrt{s_{NN}} = 19.6$ and 130 GeV and from the 2001 Au + Au run at $\sqrt{s_{NN}} = 200$ GeV. The PHOBOS apparatus (Fig.1) used during this period consists of silicon detectors, and plastic detectors. The silicon detectors are employed for vertex finding, particle tracking and multiplicity measurements [3, 2]. The multiplicity detector has nearly full azimuthal coverage over a large pseudorapidity range $|\eta| < 5.4$, and the the two-arm spectrometer covers $0.5 \leq \eta \leq 1.5$. Each arm of the spectrometer has a total of 16 planes of silicon sensors located on either side of the beam pipe. The spectrometer arms are placed between the poles of a magnet which provides a field of 2 T for momentum measurements. The trigger signals are provided by sets of "plastic" detectors: the "cerenkov"counters, the "paddle" scintillator counters and by the zero degree calorimeters [4–6]. They provide the primary event and the vertex selection.

2. Global Observables

Figure 2 summarizes all the multiplicity measurements taken by PHOBOS, the pseudorapidity distribution of primary charged particles produced in Au + Au collisions at, $\sqrt{s_{NN}} = 19.6$, 130 and 200 GeV, for a range of collision centralities. The details of the analysis procedures can be found in Ref. [7].The centrality of the collisions is characterized by the average number of participants (N_{part}). For the 130 and 200 GeV data sets this was estimated from the data using the paddle counters, two sets of 16 plastic counters covering $3 < |\eta| < 4.5$ forward and backward of the interaction point. The truncated mean of the adc signals from the paddle counters is proportional to the charged multiplicity in the acceptance region of the these counters . N_{part} then is extracted for a given fraction of the cross-section from the multiplicity of the paddles, given that this multiplicity increases monotonically with the centrality. The monotonic relation between the truncated mean and N_{part} was verified using the correlations of the paddles and the zero degree calorimeters. The calculation of N_{part} and the discussion of the associated systematic errors is

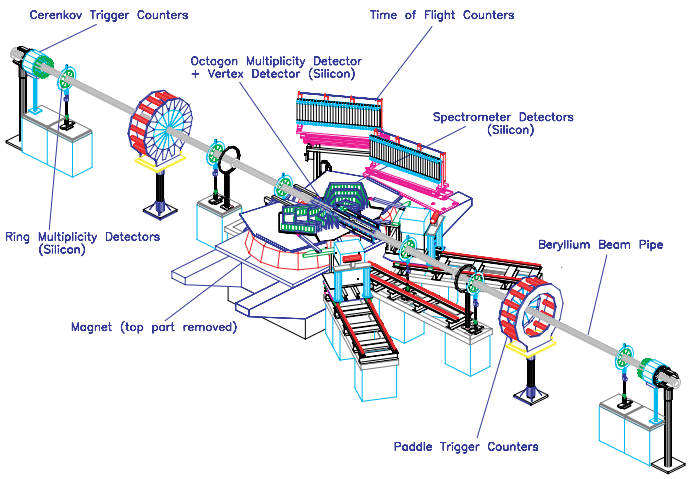

Fig. 1. PHOBOS apparatus

outlined in Ref [8]. For the lowest energy data set, the lower beam rapidity precludes use of the same method to calculate the centrality, instead a different quantity was constructed "EOCT", which is proportional to the multiplicity, that is the path-length corrected sum of the energy deposited in the octagon (silicon) detector. As for the paddle counters, it is only assumed that EOCT varies monotonically with N_{part}.

2.1. Limiting Fragmentation and Scaling

Taking advantage of the large pseudo rapidity coverage PHOBOS can study the properties of the multiplicity distributions in the fragmentation region. This is done by looking at the data from different energies in the appropriate rest frame of the colliding nuclei. For reference, in $p\bar{p}$ systems, at high enough collision energy, the multiplicity reaches a limiting value becoming independent of the energy at $y' = 0$ ($y' = y - y_{beam}$), this behavior is referred as "limiting fragmentation" and has been found to be valid for pp and pA collisions. The limiting value of $d^2N/dy'dp_t$ implies limiting value of $dN/d\eta'$ where $\eta' = \eta - y_{beam}$.

Figure 3 shows the scaled, shifted pseudorapidity distributions $dN_{ch}/d\eta'/\langle N_{part}/2\rangle$ for central Au + Au collisions which span a factor of ten in collision energy ($\sqrt{s_{NN}}$). The distributions are scaled by $\langle N_{part}/2\rangle$ to remove the effect of the different number of nucleons participating in collisions with different centralities. The results are folded about mid-rapidity (positive and negative η bins are averaged). The distributions are observed to be independent of collision energy over a substantial η' range. This result is in contrast with boost-invariance scenarios which predict a fixed fragmentation region and a central rapidity plateau that grows with increasing

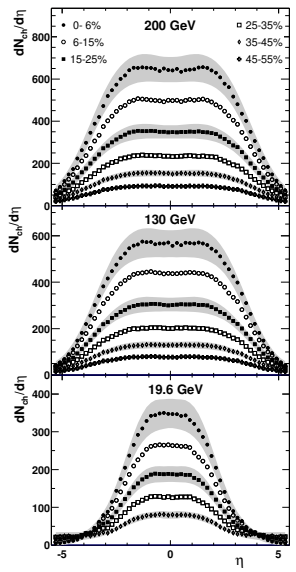

Fig. 2. The charged particle pseudorapidity distribution, $dN_{ch}/d\eta$, measured for Au + Au at $\sqrt{s_{NN}}$ = 200, 130, and 19.6 GeV for the specified centrality bins. These bins range from 0–6% central to 45–55% in the case of the higher energy data and 0–6% to 35–45% for the 19.6 GeV data. The statistical errors are negligible. The typical systematic errors (90% C.L.) are shown as bands for selected centrality bins.

energy.

A broader discussion of limiting fragmentation and PHOBOS data can be found in Ref. [9]. Here we note that it was observed that the limiting fragmentation curve changes significantly with centrality at a given energy. This is due mainly to an excess of particles at high η' for peripheral events and a narrowing of the overall distribution.

Another empirical observation derived from the multiplicity measurements is the scaling of the multiplicity distributions with N_{part}. Figure 4, shows the total charged multiplicity per participant pair as a function of the number of participants for Au + Au at three different energies. Also shown in the figure are the equivalent results for p$\bar{\text{p}}$ and e^+e^- systems at the same value of $\sqrt{s}$. The total multiplicity in Au + Au scales approximately with the number of participants (wounded nucleons), the total particle production in Au + Au is the same as the production for e^+e^- at the same energy for a broad range of centralities, on the other hand the production for p$\bar{\text{p}}$ is reduced, when compared to Au + Au. A detailed discussion on this scaling behavior is found in Ref [10].

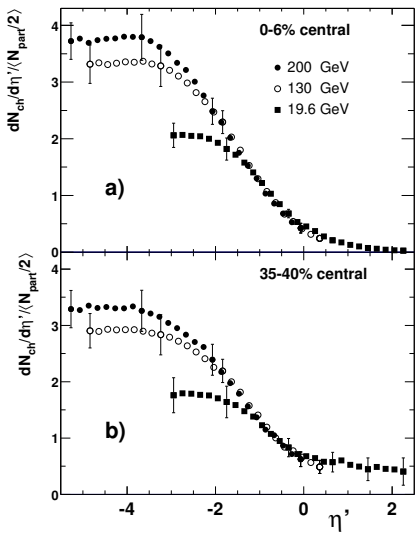

Fig. 3. Au + Au data for $\sqrt{s_{NN}} = 19.6$, 130, and 200 GeV, plotted as $dN_{ch}/d\eta'$ per participant pair, where $\eta' \equiv \eta - y_{beam}$ for a) 0–6% central, b) 35–40% central. Systematic errors (90% C.L.) are shown for selected, typical, points.

2.2. Particle Ratios

The PHOBOS spectrometer was used to measure the multiplicity ratios of anti-particles to particles. The results are shown in Table 1, as a function of the particle type and energy. These results are for the 12 % most central Au + Au collisions. A steep increase occurs for the anti proton to proton ratio from 130 GeV to 200 GeV this suggests a rapidly decreasing net-baryon density near mid rapidity with increasing energy. Also, from the measurement of the anti-kaons to kaons ratio, using a statistical model and a temperature T_{ch} of 160 - 170 GeV, the baryon chemical potential was found to be 45 ± 5 MeV at 130 GeV to 27 ± 2 MeV at 200 GeV. The details of the analysis can be found in Ref. [11,12], where it is also shown that for the 200 GeV data set the ratios, within errors, seem constant when plotted as function of p_t and N_{part}.

2.3. Low p_t spectra

One of the unique capabilities of the PHOBOS spectrometer is the identification of particles with low transverse momentum. In order to extend the identification of such particles to the lowest energy, we require that they stop in the fifth Si

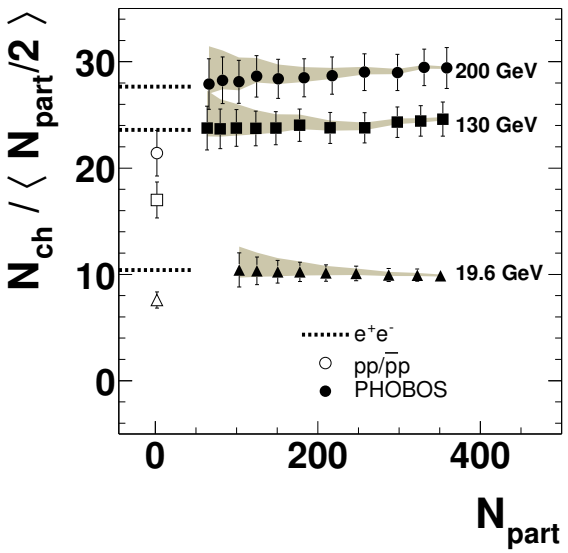

Fig. 4. $\langle N_{ch}\rangle/\langle N_{part}\rangle$ is shown vs. N_{part} for $\sqrt{s_{NN}}$ = 19.6, 130, and 200 GeV as closed symbols. The error includes contributions from the uncertainty on overall N_{ch} scale and N_{part} scale. The shaded band shows the uncertainty on the extrapolation procedure. The open symbols show UA5 data at 200 GeV and results from an interpolation for the lower energies. The dotted lines show the values from the e^+e^- fit.

plane of the spectrometer. That is, we look for tracks with large energy depositions in the first five planes. The current estimates of the systematic uncertainties for this measurement are ±20% for pions, ±40% for kaons and ±50% for protons. A detail description of this analysis is in [13]. Figure 5 shows preliminary results for invariant yields of $\pi^{\pm}$, $K^{\pm}$ and $p+\overline{p}$ measured at mid-rapidity in the transverse momentum ranges from 30 to 50 MeV/c for charged pions, 90 to 130 MeV/c for kaons and 140 to 210 MeV/c for protons and anti-protons for the 15% most central Au+Au collisions at $\sqrt{s_{NN}}$ = 200 GeV. When we put this measurement together with results at high p_t from other experiments [14], it becomes clear that there is no enhancement in the low p_t yields, and it is observed that the yields of $p+\overline{p}$ agree with the extrapolation of the PHENIX measurements at higher p_t [14], indicating that the flattening of proton spectra attributed to the collective radial expansion extends down to very low transverse momentum.

2.4. High p_t spectra

In Figure 6 we present the invariant cross-section of charged hadrons, averaging the yields of positive and negative hadrons as a function of transverse momentum. Data are shown for 6 centrality bins, ranging from$\langle N_{part}\rangle = 58$ to $\langle N_{part}\rangle = 344$. We see that all spectra exhibit a smooth drop-off with a slightly concave shape. Details of the analysis and a broader discussion of the high p_t spectra are in Ref. [15].

The detailed evolution of the shape is shown in Fig. 7, where we have divided the 6 spectra by a factor $\langle N_{part}\rangle \times f(p_T)$, where $f(p_T)$ is a fit of the invariant cross-section in proton-antiproton collisions at $\sqrt{s_{NN}} = 200$ GeV [16]. We observe little change in the spectral shape comparing the most peripheral to the most central collisions.

Finally Figure 8 shows the relative yield of charged hadrons in Au+Au and proton-antiproton collisions at $p_t = 0.5$, 1.5 and 3 GeV/c. The ratio was determined by interpolating the data shown in Fig. 6 using power law fits. Over the centrality range covered in this analysis, the yields at all values of p_t show very close scaling with N_{part}. This is in contrast to the expectation that particle production should be characterized by a change from $\langle N_{part}\rangle$ scaling at low p_t to $\langle N_{coll}\rangle$ scaling at high p_t.

Acknowledgment

This work was partially supported by U.S. DOE grants DE-AC02-98CH10886, DE-FG02-93ER40802, DE-FC02-94ER40818, DE-FG02-94ER40865, DE-FG02-99ER41099, and W-31-109-ENG-38 as well as NSF grants 9603486, 9722606 and 0072204. The Polish group was partially supported by KBN grant 2-P03B-10323. The NCU group was partially supported by NSC of Taiwan under contract NSC 89-2112-M-008-024.

Table 1. Particle-antiparicle ratios for the 12 % most central Au + Au at two energies.

Ratio	$\sqrt{s_{NN}}$ (GeV)	Value	Error
$\langle K^-\rangle/\langle K^+\rangle$	130	0.91	$\pm$ 0.07(stat) $\pm$ 0.06 (syst)
$\langle \bar{p}\rangle/\langle p\rangle$	130	0.60	$\pm$ 0.04(stat) $\pm$ 0.06 (syst)
$\langle \pi^-\rangle/\langle \pi^+\rangle$	130	1.00	$\pm$ 0.01(stat) $\pm$ 0.02 (syst)
$\langle K^-\rangle/\langle K^+\rangle$	200	0.95	$\pm$ 0.03(stat) $\pm$ 0.03 (syst)
$\langle \bar{p}\rangle/\langle p\rangle$	200	0.73	$\pm$ 0.02(stat) $\pm$ 0.03 (syst)
$\langle \pi^-\rangle/\langle \pi^+\rangle$	200	1.025	$\pm$ 0.006(stat) $\pm$ 0.018 (syst)

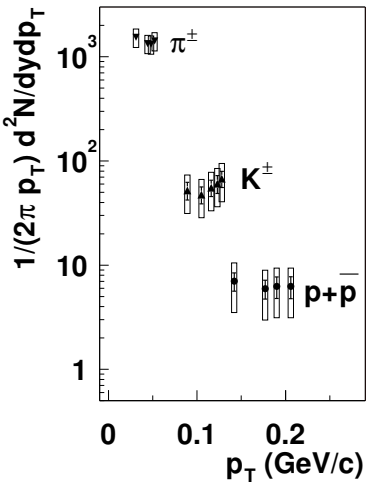

Fig. 5. Invariant yields as a function of p_t. The boxes show systematic uncertainties.

Note(s)

a. Corresponding Author:
Physics Department M/C 273,
University of Illinois at Chicago,
Chicago IL 60607
E-mail: ejgarcia@uic.edu

References

1. J.P. Blaizot, *Nucl. Phys.* **A661** (1999) 3.
2. Pernegger H et al. *Nucl. Inst. Meth.* **A419** (1998) 549
3. Back B et al. *Nucl. Inst. Meth.* **A447** (2000) 257
4. R. Bindel, E. Garcia, A.C. Mignerey and L.P. Remsberg, *Nucl. Inst. and Meth* **A**474 (2001)38.
5. R. Bindel, R. Baum, E. Garcia, A.C. Mignerey and L.P. Remsberg, *Nucl. Inst. and Meth* **A**488 (2002)94.
6. C. Adler, A. Denisov, E. Garcia, M.Murray, H. Strobele and S.White *Nucl. Inst. and Meth.* **A**470 (2001)488.
7. B.B. Back *et. al.*, Phys. Rev. Lett. **87**, 102303 (2001).

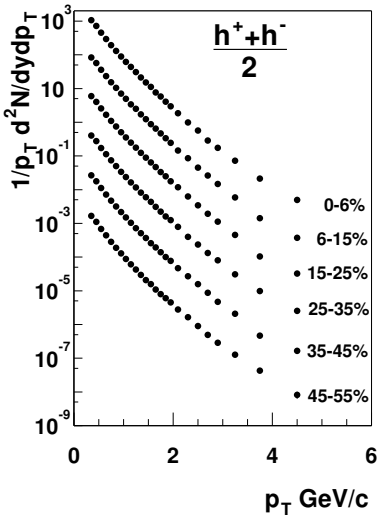

Fig. 6. Invariant yields for charged hadrons as a function of p_t for 6 centrality bins. For clarity, consecutive bins are scaled by factors of 10.

8. B. B. Back *et. al.*, Phys. Rev. C**65**, 061901R (2002).
9. B.B Back *et. al.*, nucl-ex/0210015 Oct 2002 - PRL (submitted)
10. B.B. Back *et. al.*, nucl-ex/0301017 Jan 2003.
11. B.B. Back *et. al.*, Phys. Rev. Lett. **87**, 102301 (2001).
12. B.B Back *et. al.*, nucl-ex/0301017 March 2003 - PRL (submitted)
13. B.B Back *et. al.*, nucl-ex/0210037 July 2003.
14. T.G. Ullrich *et. al.*, nucl-ex/0211004 to be published in QM2002 proceedings.
15. B.B Back *et. al.*, nucl-ex/0210006 Oct. 2002 - PRL (submitted)
16. C. Albajar *et al.*, Nucl. Phys. **B335**, (1990) 261.

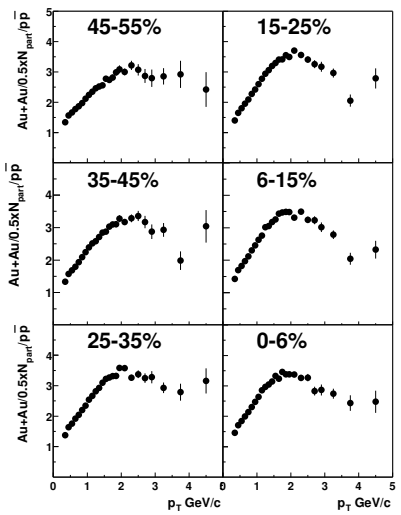

Fig. 7. Ratio of the charged hadron yield in Au+Au relative to proton-antiproton collisions scaled by $0.5 \times \langle N_{part} \rangle$ as function of p_T for 6 centrality bins.

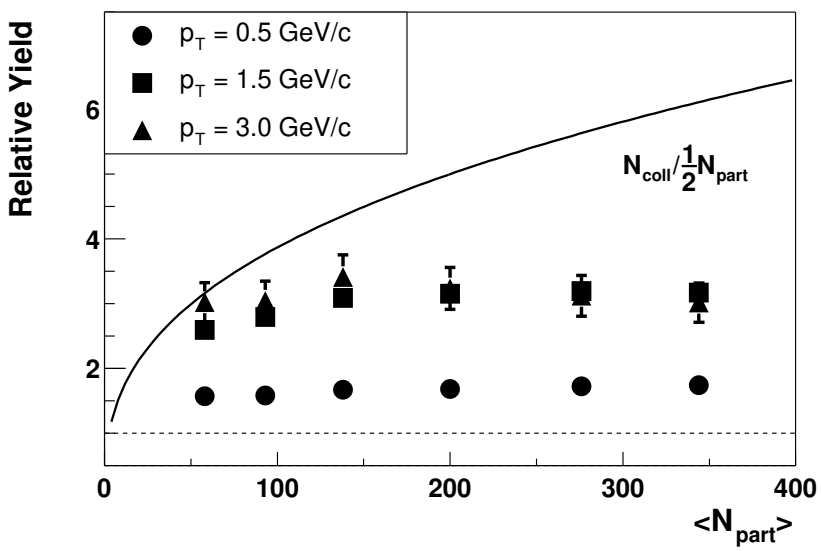

Fig. 8. Ratio of the charged hadron yield in Au+Au relative to proton-antiproton collisions scaled by $0.5 \times \langle N_{part} \rangle$ at p_T = 0.5, 1.5 and 3 GeV/c. The solid line shows the ratio of the number of binary collisions to number of participants from a Glauber calculation.